NASA TN D-466

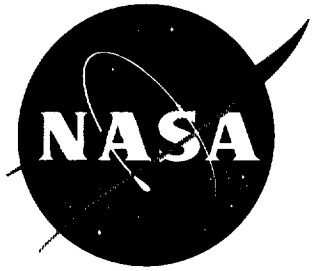

TECHNICAL NOTE

D-466

A GRAPHICAL METHOD FOR ESTIMATING

ION-ROCKET PERFORMANCE

By Thaine W. Reynolds and J. Howard Childs

Lewis Research Center
Cleveland, Ohio

NATIONAL AERONAUTICS AND SPACE ADMINISTRATION

WASHINGTON

August 1960

NATIONAL AERONAUTICS AND SPACE ADMINISTRATION

TECHNICAL NOTE D-466

A GRAPHICAL METHOD FOR ESTIMATING ION-ROCKET PERFORMANCE

By Thaine W. Reynolds and J. Howard Childs

SUMMARY

Equations relating the critical temperature and ion current density for surface ionization of cesium on tungsten are derived for the cases of zero and finite electric fields at the ion-emitting surface. These equations are used to obtain a series of graphs that can be used to solve many problems relating to ion-rocket theoretical performance. The effect of operation at less than space-charge-limited current density and the effect of nonuniform propellant flux onto the ion-emitting surface are also treated.

INTRODUCTION

The potential of the ion rocket as a space propulsion engine (for example, refs. 1 and 2) has led to a sizable research and development program on this engine. This work is being conducted in both the NASA Lewis Research Center (ref. 3) and in several laboratories in industry. A method for estimating the performance to be expected with various ion-rocket configurations at different operating conditions is therefore of importance.

Figure 1 depicts one simple ion-rocket configuration wherein a contact ion source is employed. Many of the concepts and terminology that follow can be understood by reference to this figure.

The type of ion source receiving the greatest research attention for possible ion-rocket application is the contact ionization of alkali metals, primarily cesium, on heated surfaces having a high electron work function, primarily tungsten. This report presents a graphical method for estimating the performance of those ion rockets that employ contact ionization of cesium on tungsten surfaces. The relations on which the graphs are based were obtained from theory and from analysis of reported data on contact ionization. The various assumptions and limitations that apply to the method are listed in a subsequent section of the report. The report also considers the effect on efficiency of nonuniform current density and of operation at current densities below the space-charge-limited condition.

SYMBOLS

A	ion-emitting area, m^2
E	electric-field strength, v/m
h	distance of propellant supply tube to emitter surface, m
I_s	specific impulse, sec
j	ion current density, amp/m^2
j_{av}	average ion current density over total emitter area, amp/m^2
j_{ideal}	ion current density for ideal diode, amp/m^2
j_{max}	maximum local ion current density, amp/m^2
k	Boltzmann constant
L	accelerator length, m
m	ion mass, kg
P_A	power input to accelerator electrode, w
P_B	ion beam power, w
P_{elect}	power required to emit electrons, w
P_{gen}	power input to ion rocket from generator, w
P_{prop}	power required to vaporize and ionize propellant, w
$\sum P_{loss}$	summation of power losses from ion rocket, w
P_R	power radiated from ion emitter, w
Q_R	energy loss by radiation from ion source, ev/ion
q	electronic charge, coulomb
T	ion emitter temperature, ^oK
V	voltage, v
V_e	voltage at ion emitter, v

ERRATA

NASA TECHNICAL NOTE D-466

By Thaine W. Reynolds and J. Howard Childs

August 1960

E-822

Page 18: Replace figure 2(c) with the figure on the reverse side of this sheet.

Issued 5-3-61

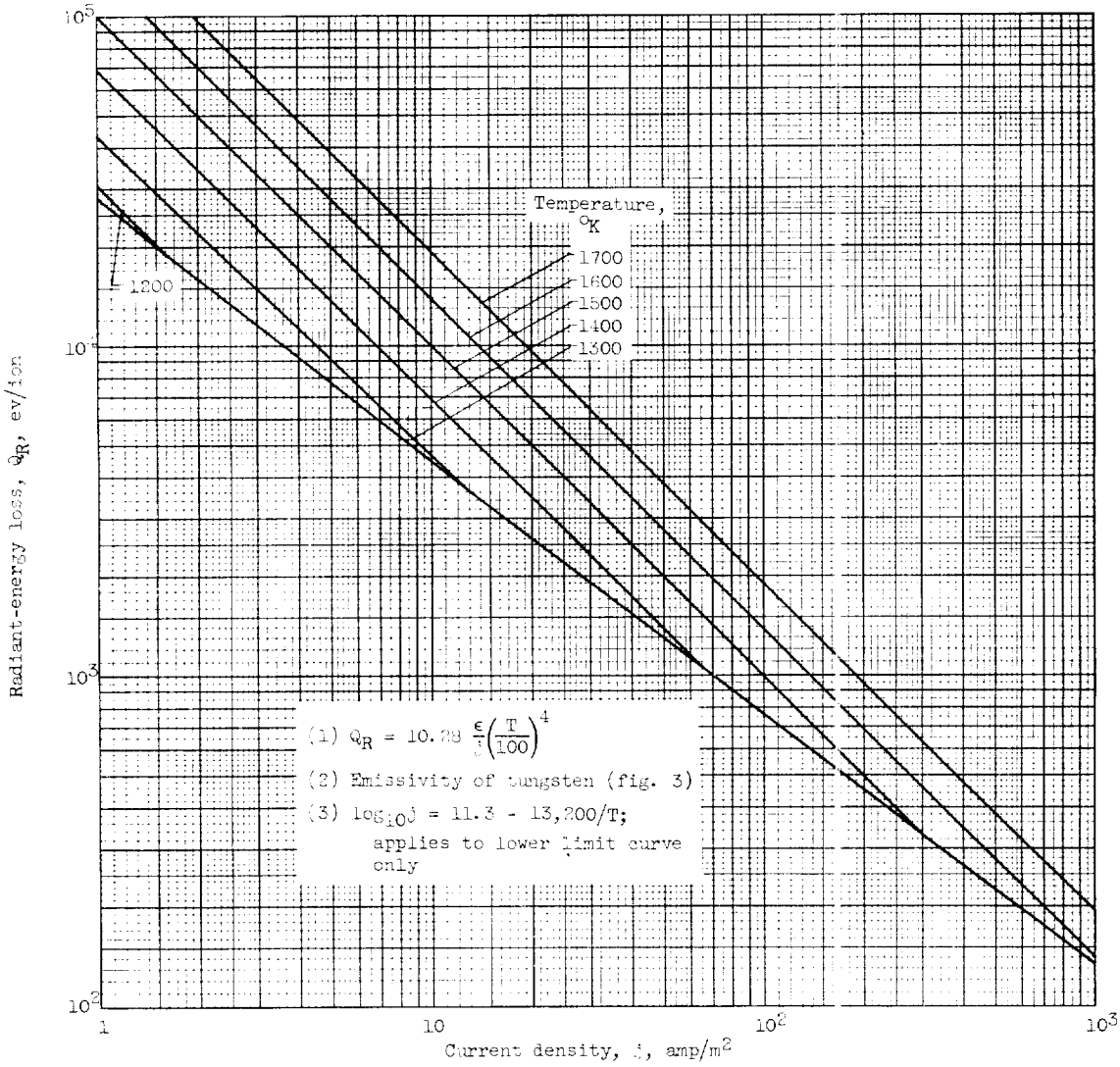

(c) Radiant-energy loss.

Figure 2. - Continued. Graphs for determining ion-rocket-engine performance.

ΔV_A voltage drop across accelerating gap, v

ΔV_T overall voltage drop, v

W_e width of emitter surface, m

X fractional distance from emitter edge

Z ratio of beam power to radiated power at two conditions (defined by eq. (31))

ϵ thermal emissivity

ϵ_0 permittivity of free space

η ion-rocket energy efficiency

η_s energy efficiency of ion source (uniform flux)

η_δ energy efficiency of ion source (nonuniform flux)

φ potential energy, ev

EQUATIONS FOR ION-ROCKET EFFICIENCY

Ion-rocket energy efficiency is given by:

$$\eta = \frac{P_B}{P_B + \sum P_{loss}} = \frac{P_B}{P_{gen}} \tag{1}$$

The various components of the term $\sum P_{loss}$ for an ion rocket employing a contact ion source are as follows:

P_R The radiated power from the hot tungsten surfaces. This is by far the largest part of $\sum P_{loss}$ in most engines using contact ion sources. For a given P_R, the value of P_B attainable is dependent on the uniformity of the propellant flux onto the ionizing surface; this will be further discussed.

P_{prop} The power required to vaporize and ionize the propellant. This is usually negligible: $P_{prop} < 6J$, watts, where J is total current in amperes.

P_{elect} The power required to emit the electrons for beam neutralization. The value of this term can range from very small to very large values relative to the other power losses, depending on the electron emitter configuration and work function (hence, temperature).

P_A The power required to maintain electric potential on the engine electrodes. This term must be very small in any engine having reasonable operating life, since ion impingement on the electrodes or electron emission from the electrodes would result in severe erosion and/or overheating of engine parts.

Of the various component terms in $\sum P_{loss}$, only P_R is included in the computations and graphs that follow. The term P_R is associated with the ion source, while the other $\sum P_{loss}$ component terms are associated with other parts of the engine. In the strict sense, therefore, the following discussion deals with the ion-source energy efficiency η_s:

$$\eta_s = \frac{P_B}{P_B + P_R} \tag{2}$$

As just noted, the other terms in $\sum P_{loss}$ may prove to be negligible for many ion rockets, in which case

$$\eta_s \approx \eta \tag{3}$$

Many of the equations that follow apply only to η_s; others apply also to η, and in such cases the appropriate symbols are used.

GRAPHS FOR ION-ROCKET PERFORMANCE

Most of the equations for ion-rocket theoretical performance are well documented (e.g., ref. 3); derivations of these equations are not repeated herein. Except when otherwise noted, the equations that follow are included in, or can be easily derived from, those of reference 3.

Performance with Uniform Propellant Flux

For cases where propellant flux onto the ionizing surface is uniform, figure 2 permits a graphical determination of various performance parameters, including η_s. Figure 2 contains four page-size graphs that can be used to determine ion-rocket theoretical performance characteristics. Using figure 2(a), the overall voltage ΔV_T required to

yield a given specific impulse is determined. Using figure 2(b), for a given accelerator length L and accelerating voltage ΔV_A, the ideal current density j_{ideal} can be read from the abscissa. This value of j_{ideal} can be used to enter figure 2(c), where j and emitter surface temperature T serve to determine Q_R, the radiant-energy loss from the emitter in units of electron volts per ion. The lower boundary curve results from the minimum permissible temperature of operation for the emitter surface governed by the current-critical temperature relation, equation (7). The value of Q_R can then be used to enter figure 2(d), where Q_R, together with the overall voltage drop ΔV_T previously obtained, serves to determine η_s; η_s is the ion-source energy efficiency for the ion rocket giving the I_s specified in figure 2(a). A graph containing all four parts of figure 2 on a single sheet is included in addition to the page-size graphs of parts (a) to (d). This arrangement of the four parts facilitates their use.

The various parts of figure 2 are subject to the following assumptions and limitations:

(1) The propellant is cesium. (Figs. 2(a) to (c).)

(2) The ion-emitting surface is tungsten with emissivity given by figure 3. (Fig. 2(c).)

(3) Operation is at the critical temperature defined by equation (7). (Fig. 2(c).)

(4) Current density is equal to that for space-charge-limited current from an ideal plane-parallel diode of spacing L. In some cases this assumption can be modified by techniques to be discussed in a later section. (Fig. 2(b).)

(5) Thermal radiation occurs only from the ion-emitting surface. This implies complete radiation shielding on the upstream face of the emitter and zero shielding downstream. (Fig. 2(c).)

(6) Space charge limitations occur only at emitter. (Figs. 2(b) and (c).)

The essential equations used in obtaining the graphs of figure 2 are as follows:

Graph (a):

$$I_s = 123\sqrt{\Delta V_T} \tag{4}$$

Graph (b):

$$j = 0.475 \times 10^{-8} \frac{(\Delta V_A)^{3/2}}{L^2} \tag{5}$$

Graph (c):

(1) $$Q_R = 10.28 \frac{\epsilon}{j} \left(\frac{T}{100}\right)^4 \tag{6}$$

(2) Emissivity of tungsten as a function of temperature as given by figure 3

(3) $$\log_{10} j = 11.3 - \frac{13,200}{T} \tag{7}$$

(Derivation of this equation discussed in later section of report)

Graph (d):

$$\eta = \frac{P_B}{P_B + P_R} = \frac{1}{1 + \frac{P_R}{P_B}} = \frac{1}{1 + \frac{Q_R}{\Delta V_T}} \tag{8}$$

If aperture and space charge effects are known for a particular ion rocket so that $j \neq j_{ideal}$, this correction can be applied on the abscissa of figure 2(c) before determining Q_R. For grid electrodes the values of j/j_{ideal} can be estimated by the method of reference 4 (see also ref. 5). For other electrode configurations, j/j_{ideal} can often be determined from limited test data on the particular engine under consideration.

Performance with Nonuniform Propellant Flux

In some ion rockets a nonuniform propellant flux onto the ion-emitting surface may be encountered. With porous tungsten emitters this might result from nonuniform porosity. In other contact ion sources it might result from the pattern of flux out of the propellant vapor supply system. One example of nonuniform propellant flux is shown in figure 4; this is the computed flux pattern for the engine depicted in figure 1.

Where a nonuniform propellant flux exists, the ion emitter temperature must be maintained at the critical temperature corresponding to the local j_{max}. Otherwise, an adsorbed cesium layer will build up

at that location with the resulting emission of a large percent of neutral cesium atoms. Thus, while T and P_R are fixed by j_{max}, the value of P_B is reduced from the value that would be obtained if j were uniform across the emitter with $j = j_{max}$. This reduction in P_B results in a lower value of η_s and η.

In figure 4 the area under the curve is proportional to j_{av}, while the total rectangular area is proportional to j_{max}. Now, if η represents the energy efficiency that would be obtained with uniform propellant flux and η_δ represents the efficiency with nonuniform flux, then

$$\eta = \frac{j_{max} A \Delta V}{j_{max} A \Delta V + \sum P_{loss}} \tag{9}$$

and

$$\eta_\delta = \frac{j_{av} A \Delta V}{j_{av} A \Delta V + \sum P_{loss}} \tag{10}$$

Now, values of η (actually η_s) are obtained from figure 2, and simple correction factors are desired to use with these values to obtain η_δ and $\eta_{s,\delta}$ for cases where propellant flux is not uniform:

$$\frac{\eta_\delta}{\eta} = \frac{j_{av}/j_{max}}{\left(\frac{j_{av}}{j_{max}} - 1\right)\eta + 1} \tag{11}$$

and

$$\frac{\eta_{s,\delta}}{\eta_s} = \frac{j_{av}/j_{max}}{\left(\frac{j_{av}}{j_{max}} - 1\right)\eta_s + 1} \tag{12}$$

A plot of η_δ/η and $\eta_{s,\delta}/\eta_s$ is included in figure 5. If a given ion rocket would have efficiency η or η_s with uniform propellant flux (fig. 2), the efficiency of that same ion rocket with nonuniform flux characterized by some value of j_{av}/j_{max} is given by appropriate values of η_δ/η or $\eta_{s,\delta}/\eta_s$ from figure 5.

A comparison of the efficiency for uniform and nonuniform propellant flux can also be made readily by use of figures 2(c) and (d). Th

efficiency η is read for j_{max} as described previously. The efficiency η_s is obtained as follows: From the point in figure 2(c) corresponding to j_{max} and critical temperature (lower line), go up a constant-temperature line to j_{av}. This point gives the appropriate value of Q_R, and the efficiency η_s is then read from figure 2(d) at this value of Q_R and the appropriate ΔV_T.

CRITICAL TEMPERATURE - CURRENT RELATIONS IN CESIUM-TUNGSTEN SYSTEM

Zero Electric Field at Emitter

A different current - critical temperature relation (eq. (7)) is used in this report from that used previously (refs. 3 and 5). This equation was derived from the data of table I of reference 6 and is recommended as the relation to use for space-charge-limited flow conditions, that is, for zero electric field at the ion emitter surface. The equation relating current and temperature that previously was used was obtained from data at other than space-charge-limited flow conditions. A comparison of the equation used herein with the earlier equation at current-density levels of interest for ion-rocket engines indicates a temperature difference of around 150° K between the two equations. This difference may make considerable difference in the power radiated by the ion emitter and hence in the calculated ion-rocket efficiency.

The zero-field relation presented herein was obtained by plotting the total evaporation rate (sum of the ion and atom currents) against the fraction of a monolayer adsorbed on the surface for several constant surface temperature values (fig. 6). A discussion of the behavior of the cesium-tungsten system as governed by these total-evaporation-rate curves may be found in reference 7. In particular, it may be noted that a plot of the current at the minimum in these curves against the temperature will yield a current - critical temperature relation. The equation so obtained is

$$\log_{10} j = 11.3 - \frac{13,200}{T} \qquad (7)$$

A plot of this relation is shown in figure 7.

Electric Field at Emitter

The existence of an electric field at the ion-emitting surface will affect both the current-voltage relation and the current - critical temperature relation. The question arises as to whether there is an optimum condition for operation, that is, one having the lowest ratio of radiated power P_R to ion beam power P_B. The discussion in this section is directed toward an answer to this question.

The equation for current flow between parallel planes when an electric field E exists at the emitter plane can be expressed

$$L = \frac{4}{3b^2}\left[(b\sqrt{\Delta V} - 2E^2)(b\sqrt{\Delta V} + E^2)^{1/2} + 2E^3\right] \qquad (13)$$

where

$$b = \frac{2\sqrt{2}}{\epsilon_0}\sqrt{\frac{m}{q}}\, j$$

A plot of equation (13) for cesium in the range of $\Delta V = 40{,}000$ volts and $j = 200$ amperes per square meter is shown in figure 8.

The effect of the existence of an electric field at the ion-emitting surface will be to reduce the effective potential barrier for the escape of ions and hence to increase the ion current flow, similar to the Schottky effect for electrons (ref. 8), illustrated pictorially:

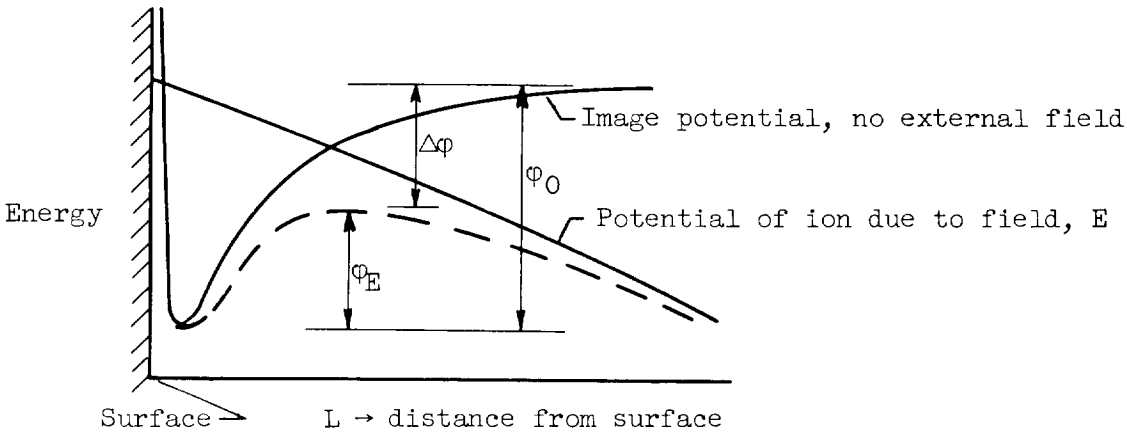

The symbol φ_0 represents the potential energy barrier to the escape of an ion in mutual interaction with the electrical image force. The amount of the reduction in the potential barrier due to the presence of the field is given by the relation

$$\Delta\varphi = -\left(\frac{qE}{4\pi\epsilon_0}\right)^{1/2} \tag{14}$$

where $\Delta\varphi$ is expressed in electron volts and E in volts per meter. Simplifying, this expression becomes

$$\Delta\varphi = -3.8\times10^{-5}\, E^{1/2} \tag{15}$$

In order to illustrate the effect of the field on ion current flow, equation (7) can be written in the form

$$j = 10^{11.3}\, e^{-2.62/kT} \tag{16}$$

In this form, from the exponential Boltzmann factor, the potential energy barrier to escape of ions at zero field would be interpreted as 2.62 electron volts.

The change in current flow caused by the field may then be given by

$$j_{E,T_0} = j_{E=0,T_0}\, e^{-\Delta\varphi/kT} \tag{17}$$

where

$j_{E=0,T_0}$ current at zero field

j_{E,T_0} current at field E and same temperature

and $\Delta\varphi$, the change in potential barrier, is given by equation (15).

An equation for current - critical temperature with other than zero electric field can be generated by using equations (15) and (17) in conjunction with the zero-field ion current relation.

Incorporating equations (15) and (17) into (16) yields the following relation for current - critical temperature at other than zero field at the emitter:

$$j = 10^{11.3}\, e^{-\frac{\varphi_0}{kT}\left(1+\frac{\Delta\varphi}{\varphi_0}\right)} \tag{18}$$

$$j = 10^{11.3}\, e^{-\frac{2.62}{kT}(1-1.45\times10^{-5}\sqrt{E})} \tag{19}$$

or, in logarithmic form, comparable with equation (7),

$$\log_{10} j = 11.3 - \frac{13,200}{T} + 0.192\,\frac{\sqrt{E}}{T} \tag{20}$$

This relation, encompassing the effect of electric field on the current critical temperature relation, may be compared with the experimental data of reference 9. In reference 9 data are presented on the effect of electric fields up to 2×10^8 volts per meter on the critical temperature for constant current. Values of $dT/d\sqrt{E}$ ranging from about -0.01° to -0.015° K/$\sqrt{\text{volt/meter}}$ were obtained.

By differentiating equation (20) at constant current, the following expression for $(\partial T/\partial\sqrt{E})_j$ is obtained:

$$\left(\frac{\partial T}{\partial\sqrt{E}}\right)_j = -\frac{1.45\times10^{-5}\,T}{1 - 1.45\times10^{-5}\sqrt{E}} \tag{21}$$

If E is limited to about 10^7 volts per meter, this relation is approximately expressed

$$\frac{dT}{d\sqrt{E}} \cong -1.45\times10^{-5}\,T \tag{22}$$

The range of temperatures investigated in reference 9 was about 700° to 900° K. In this temperature range, values of equation (22) vary from about -0.01° to -0.013° K/$\sqrt{\text{volt/meter}}$, which is in agreement with the experimentally determined values.

Efficiency with Other than Zero Field at Emitter

To determine whether there is an optimum condition of operation, that is, one in which the ratio of beam power P_B to radiated power P_R is a maximum, the ratio P_B/P_R at off-space-charge conditions can be compared with that at the space-charge-limited condition

$$\frac{P_B/P_R}{P_{B,0}/P_{R,0}} = \frac{P_B/P_{B,0}}{P_R/P_{R,0}} \equiv \frac{j/j_0}{(\epsilon T/\epsilon_0 T_0)^4} = Z \tag{23}$$

where the subscript 0 represents the space-charge-limited condition.

The actual ratio of efficiencies η/η_0 will not vary as much as the function in equation (23), since

$$\frac{\eta}{\eta_0} = \frac{Z}{1 + \eta_0(Z - 1)} \tag{24}$$

With tungsten, in the temperature range of interest for surface ionization, the emissivity is proportional to temperature, so that

$$Z \equiv \frac{j/j_0}{(T/T_0)^5} \tag{25}$$

Equation (25) can be rewritten:

$$Z = \frac{1 + \frac{\Delta j}{j_0}}{\left(1 + \frac{\Delta T}{T_0}\right)^5} \tag{26}$$

The ratio Z may be readily evaluated for a constant accelerator spacing L and constant accelerating voltage ΔV. As illustrated in the following sketch, j_0 is the space-charge-limited current flow.

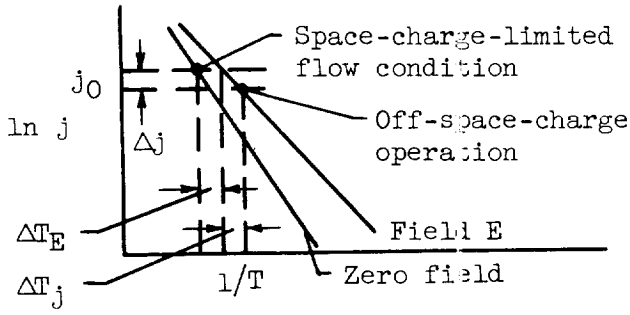

When the current is lowered by an amount Δj, a field E is present at the emitter (determined from eq. (13) or Fig. 8). The required critical surface temperature is lowered, both because of the field and because of the lowering of the current:

$$\Delta T = \Delta T_E + \Delta T_j = \frac{\partial T}{\partial \sqrt{E}} \Delta E + \left(\frac{\partial T}{\partial j}\right)\Delta j \tag{27}$$

Substituting from (22) for $\partial T/\partial\sqrt{E}$ and from equation (16) (by first differentiating) for $\partial T/\partial j$ gives

$$\frac{\Delta T}{T} = -1.45\times10^{-5}\sqrt{E} + \frac{kT}{2.32}\frac{\Delta j}{j} \tag{28}$$

and thus equation (26) can be evaluated by the relation

$$Z = \frac{1 + (\Delta j/j_0)}{\left[1 - 1.45\times10^{-5}\sqrt{E} + \frac{kT}{2.32}\left(\frac{\Delta j}{j_0}\right)\right]^5} \tag{29}$$

Values of Z have been evaluated at several sets of conditions varying from ΔV = 10,000 to 50,000 volts and currents from 200 to 1000 amperes per square meter and are shown in figure 9. According to these curves, more efficient operation could be attained at current densities a few percent below space-charge-limited values. At high current densities the region of greater efficiency for off-space-charge operation is greater.

It should be noted, however, that (1) the percentage improvement in efficiency for off-space-charge operation is small, even less than the values of Z (note eq. (24)); (2) the surface temperature lowering permitted to take advantage of this off-space-charge operation advantage is small - of the order of 50° C or less. Such close control of emitter surface temperature may be difficult.

CONCLUDING REMARKS

The graphs of ion-rocket performance parameters presented herein constitute a means for rapid determination of theoretical engine performance characteristics. The equation relating emitter temperature to space-charge-limited current density, on which the performance graphs are based, was derived from experimental data obtained with pure tungsten ion emitters in small-scale apparatus. NASA data on an experimental ion rocket (ref. 10) indicate that higher emitter temperatures are required in that engine than those indicated by this equation. This discrepancy may be due to the presence of surface impurities on the engine ion emitter. Such impurities, if present, might also alter the thermal emissivity of the emitter from that of pure tungsten. Thus, in ion-rocket experiments, the presence of impurities on the ion-emitting surface can result in radiation power losses that are greater than those computed from the equations given in this report. However, it should be possible to attain the engine performance indicated herein through the use of inerting and bake-out procedures to keep the ion emitter free of contaminants.

Lewis Research Center
National Aeronautics and Space Administration
Cleveland, Ohio, May 12, 1960

REFERENCES

1. Stuhlinger, E.: Possibilities of Electrical Space Ship Propulsion. Extract from Proc. Fifth Int. Astronautics Cong., 1954, pp. 100-119.

2. Moeckel, W. E.: Propulsion Methods in Astronautics. Int. Ser. on Aero. Sci. and Space Flight. Vol. 2, Pergamon Press, 1959, pp. 1078-1097.

3. Childs, J. H.: Design of Ion Rockets and Test Facilities. Paper No. 59-103, Inst. Aero. Sci., 1959.

4. Spangenberg, Karl Ralph: Vacuum Tubes. McGraw-Hill Book Co., Inc., 1948.

5. Childs, J. Howard, and Mickelsen, W. R.: Grid Electrode Ion Rockets for Low Specific Impulse Missions. Paper presented at Second AFOSR Symposium on Advanced Prop. Concepts, Boston (Mass.), 1959.

6. Taylor, John Bradshaw, and Langmuir, Irving: The Evaporation of Atoms, Ions, and Electrons from Caesium Films on Tungsten. Phys. Rev., vol. 44, no. 6, Sept. 15, 1933, pp. 423-458.

7. DeBoer, J. H.: Electron Emission and Adsorption Phenomena. Cambridge Univ. Press, 1935, pp. 92-93.

8. Cobine, James Dillon: Gaseous Conductors. Dover Pub., Inc., 1958.

9. Zandberg, E. Ia: Surface Ionization of Potassium Atoms and KCl and CsCl Molecules on Tungsten Filaments in Electric Fields up to 2Mv/cm. Soviet Phys.-Tech. Phys., vol. 2, no. 11, Nov. 1957, pp 2399-2409.

10. Dangle, E. E., and Lockwood, D. L: NASA Experimental Research with Ion Rockets. Paper presented at ARS Semi-Annual Meeting, Los Angeles (Calif.), May 1960.

11. Hodgman, Charles D., ed.: Handbook of Chemistry and Physics. Thirty-eighth ed., Chem. Rubber Pub. Co., 1956-1957.

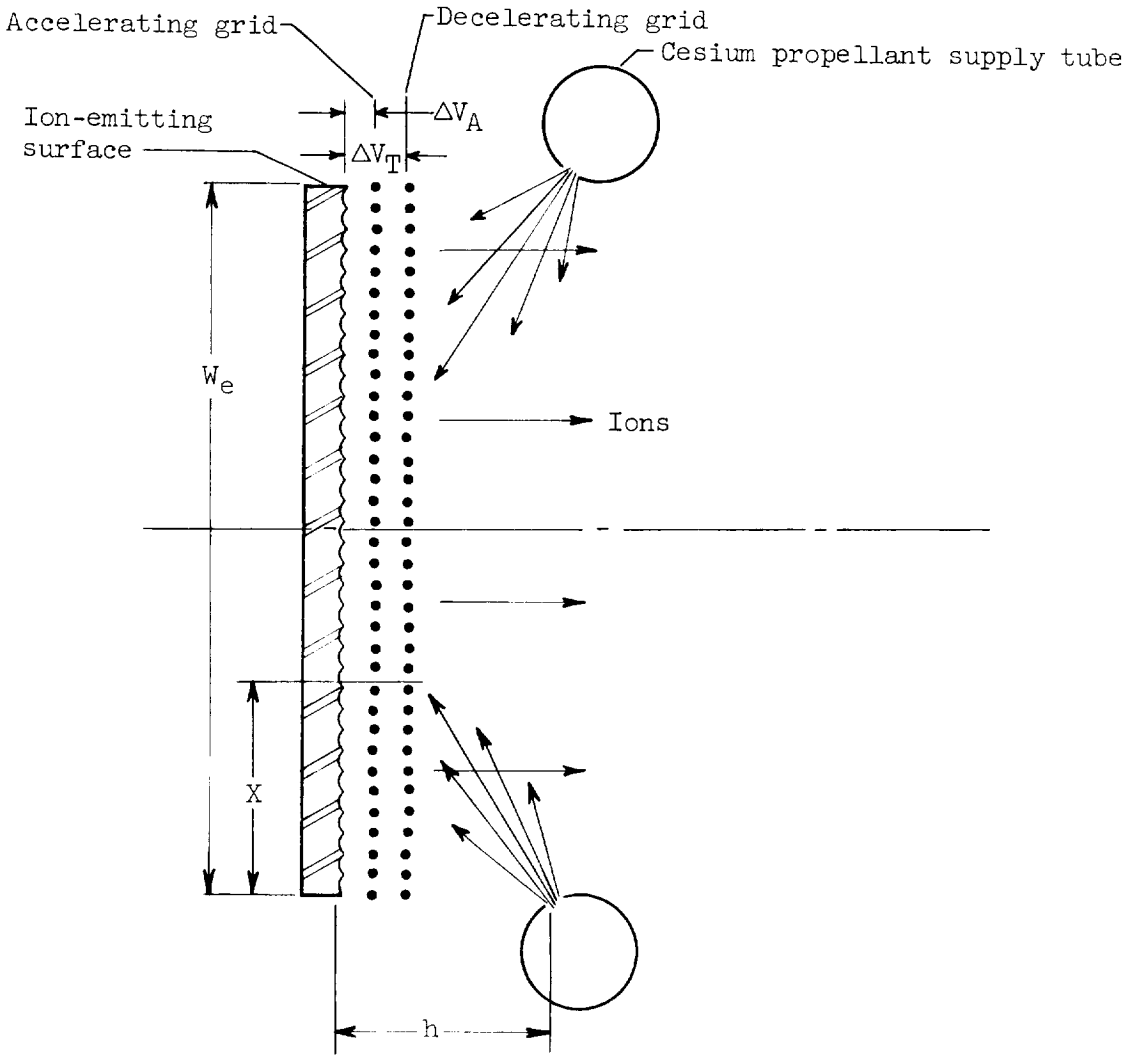

Figure 1. - Simple ion-rocket-engine configuration employing contact ion source.

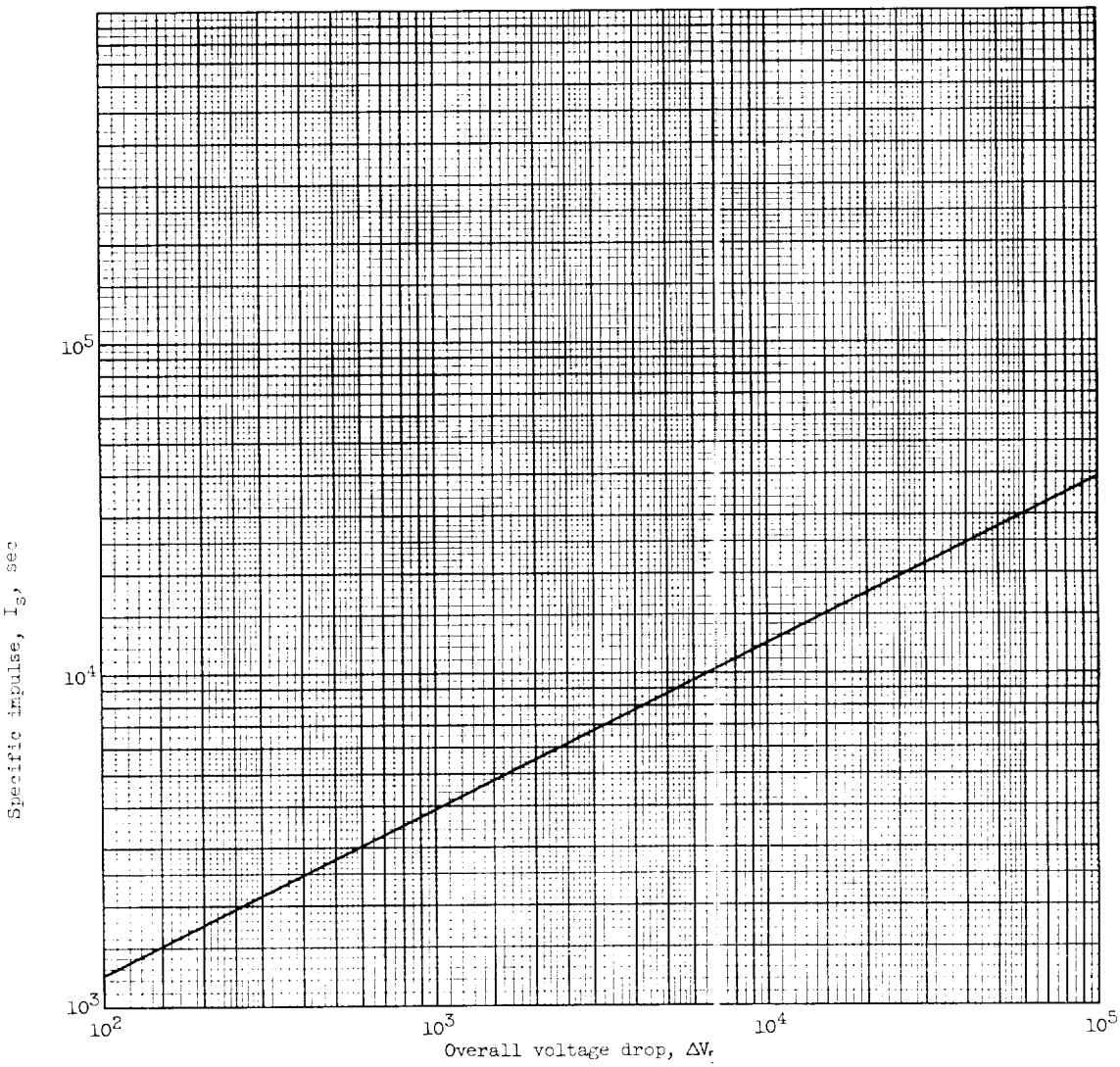

(a) Specific impulse. $I_s = 1.3\sqrt{\Delta V_T}$.

Figure 2. - Graphs for determining ion-rocket-engine performance.

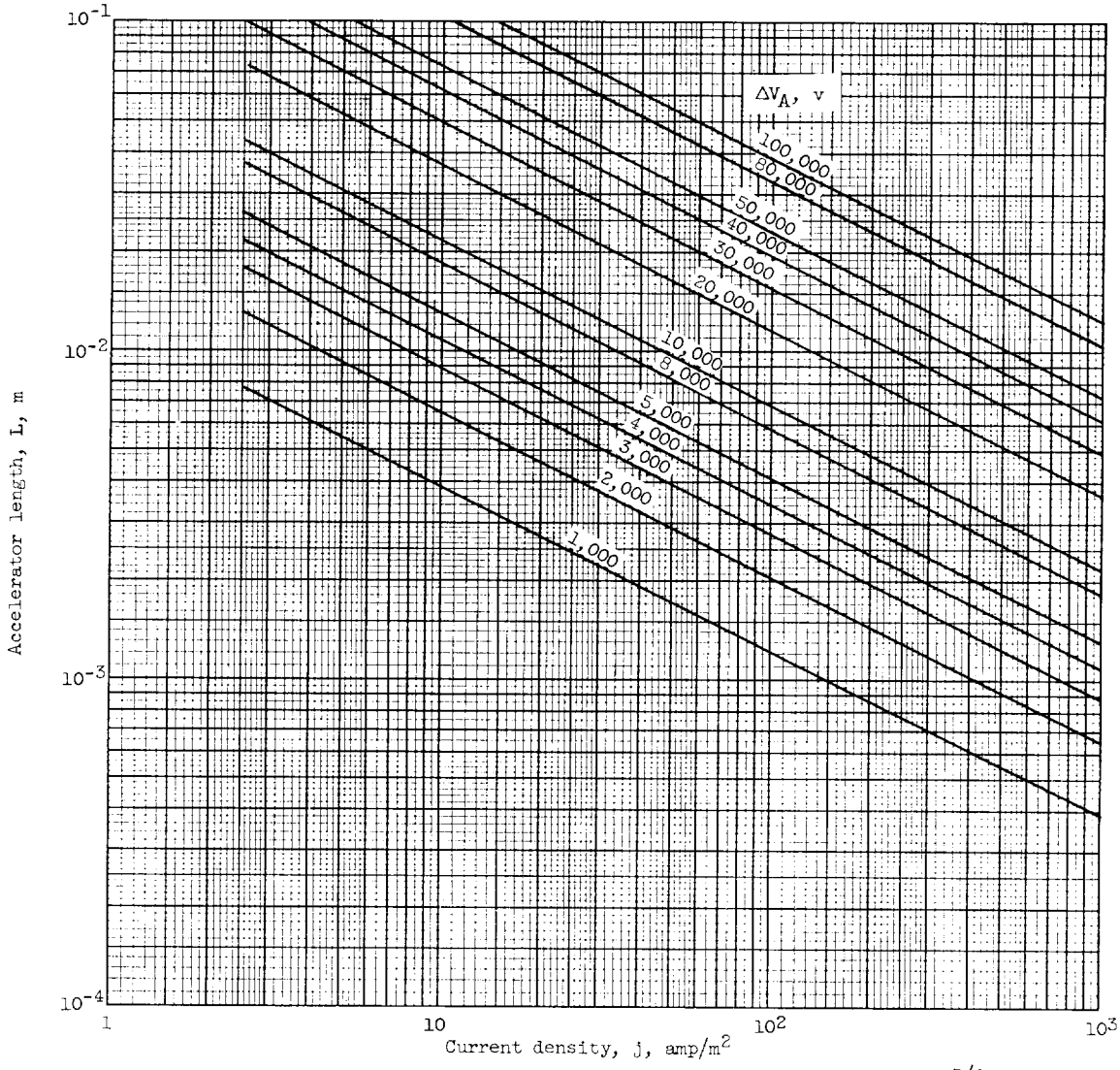

(b) Childs' law relation for plane-parallel diode. $j = 0.475 \times 10^{-8} \frac{\Delta V_A^{3/2}}{L^2}$.

Figure 2. - Continued. Graphs for determining ion-rocket-engine performance.

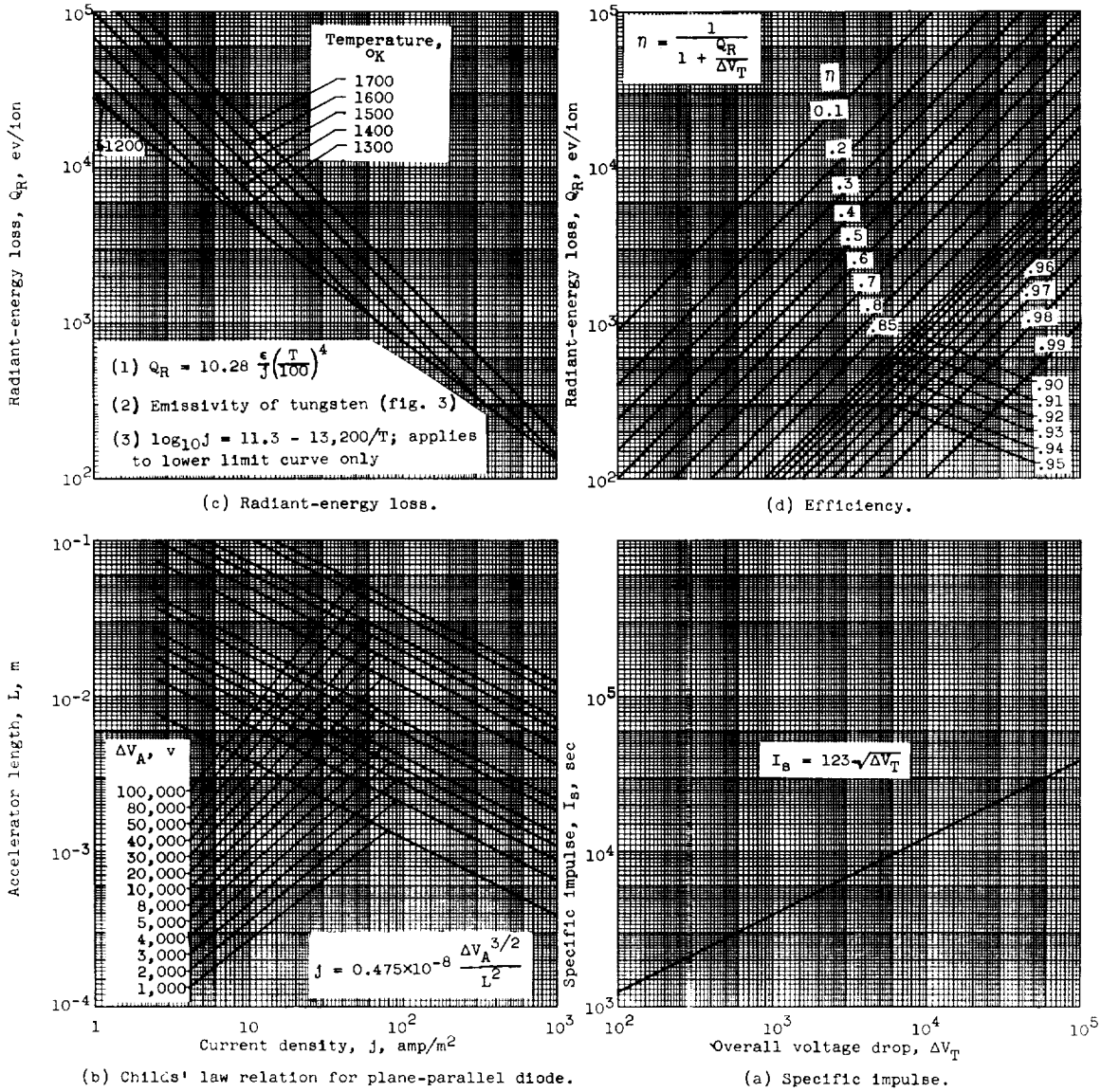

(c) Radiant-energy loss.

(d) Efficiency.

(b) Childs' law relation for plane-parallel diode.

(a) Specific impulse.

(e) Composite graph of parts (a) to (d).

Figure 2. - Concluded. Graphs for determining ion-rocket-engine performance.

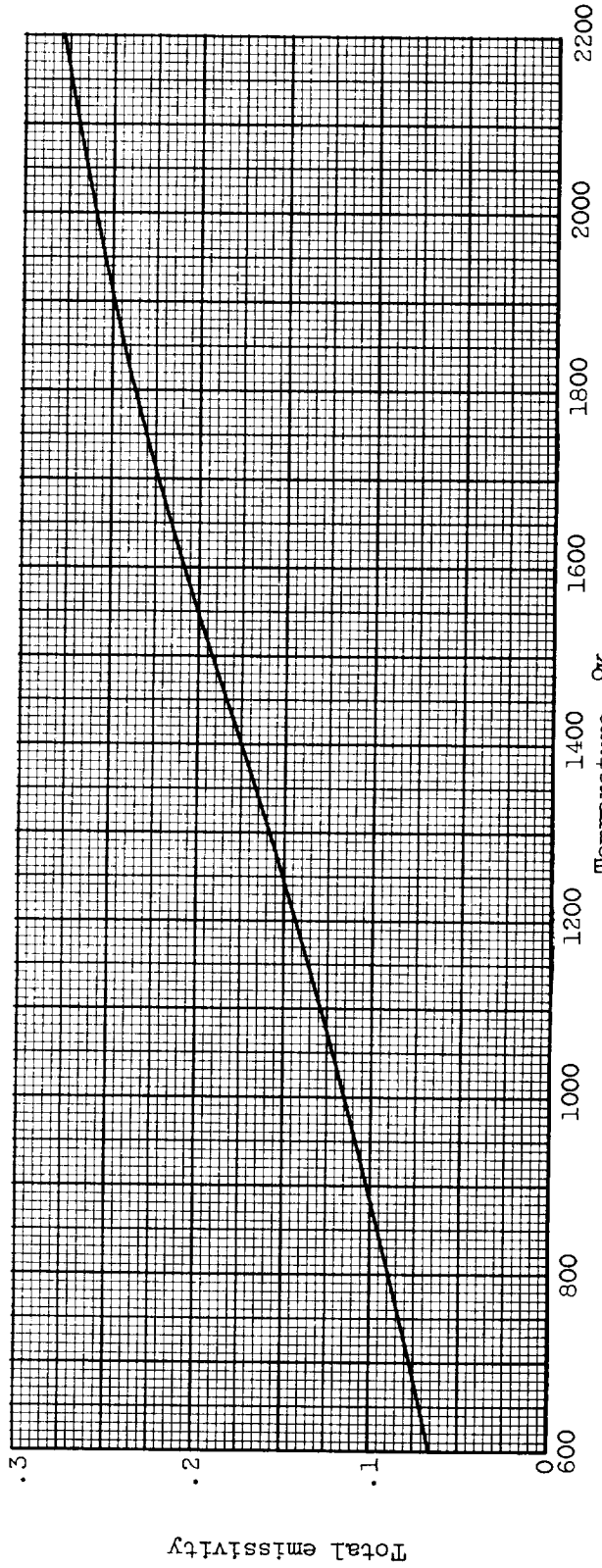

Figure 3. - Emissivity of tungsten (ref. 11).

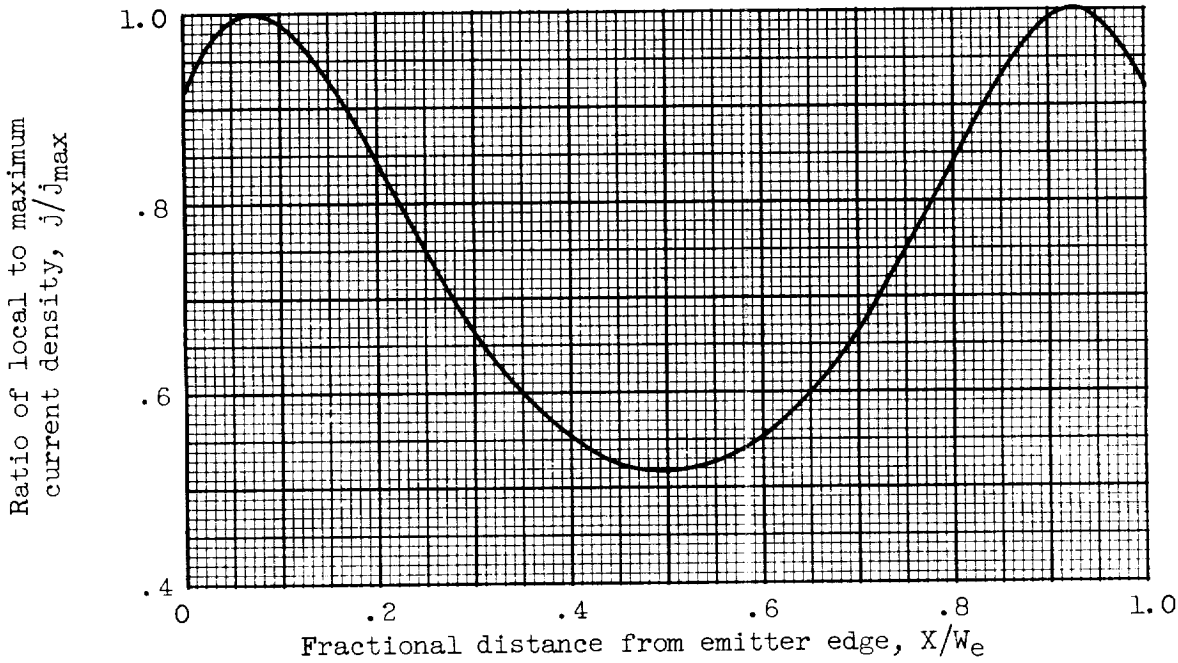

Figure 4. - Typical nonuniform current distribution pattern for engine shown in figure 1. Distance of propellant supply above emitter to emitter width, h/W_e, 0.3.

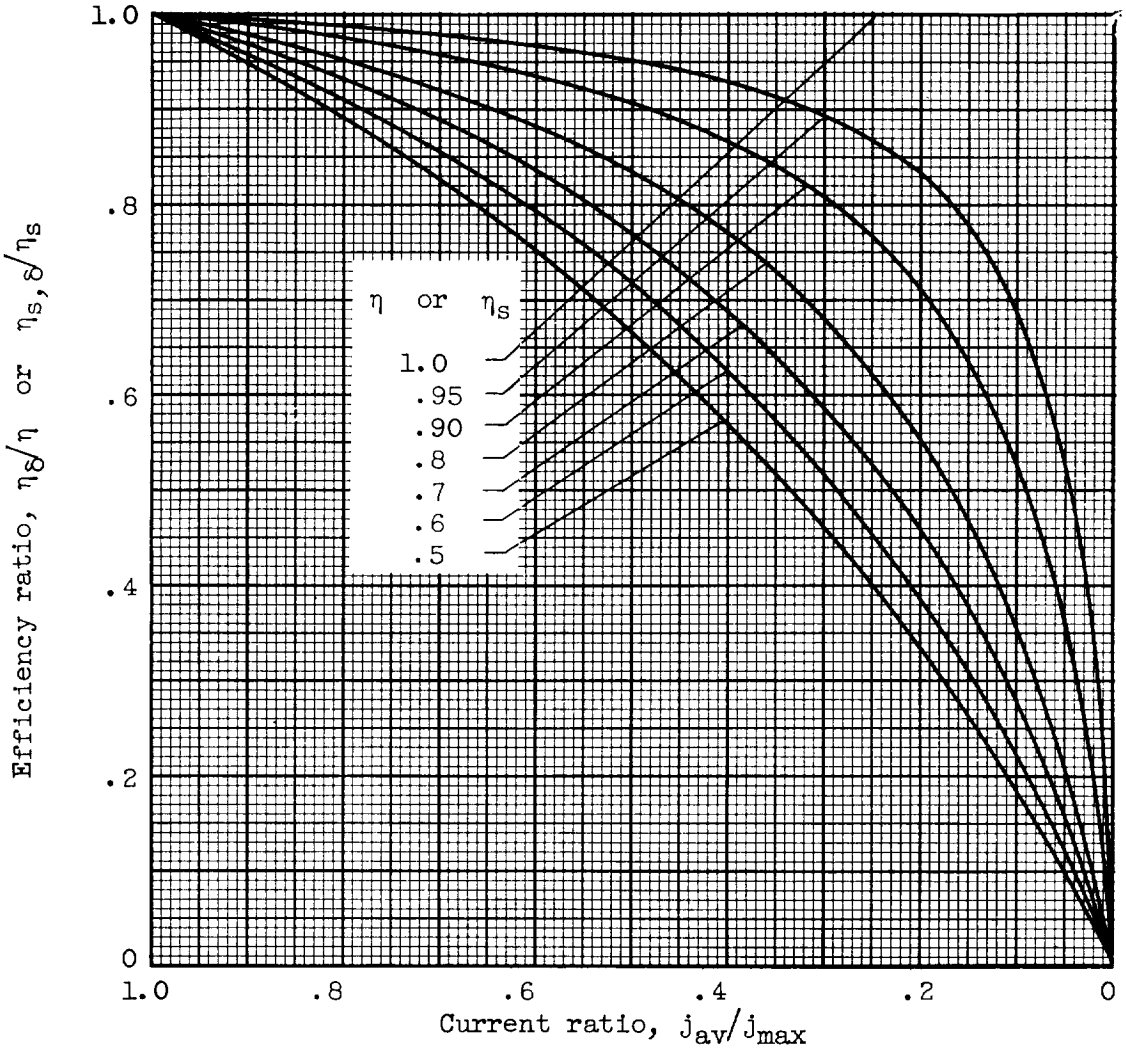

Figure 5. - Effect of nonuniform propellant flow on ion-rocket energy efficiency.

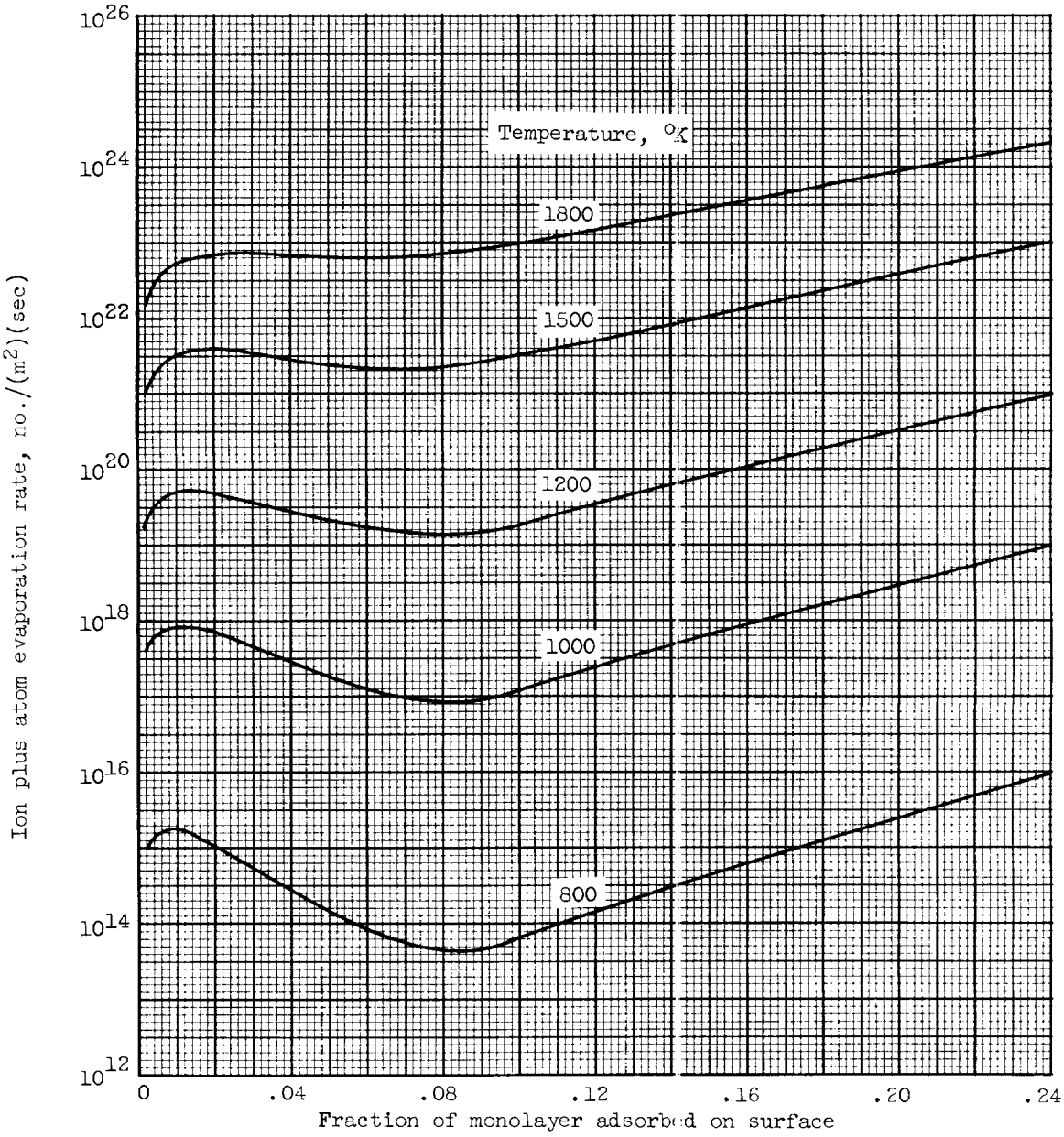

Figure 6. - Total (ion + atom) evaporation of cesium on tungsten for zero electric field at surface.

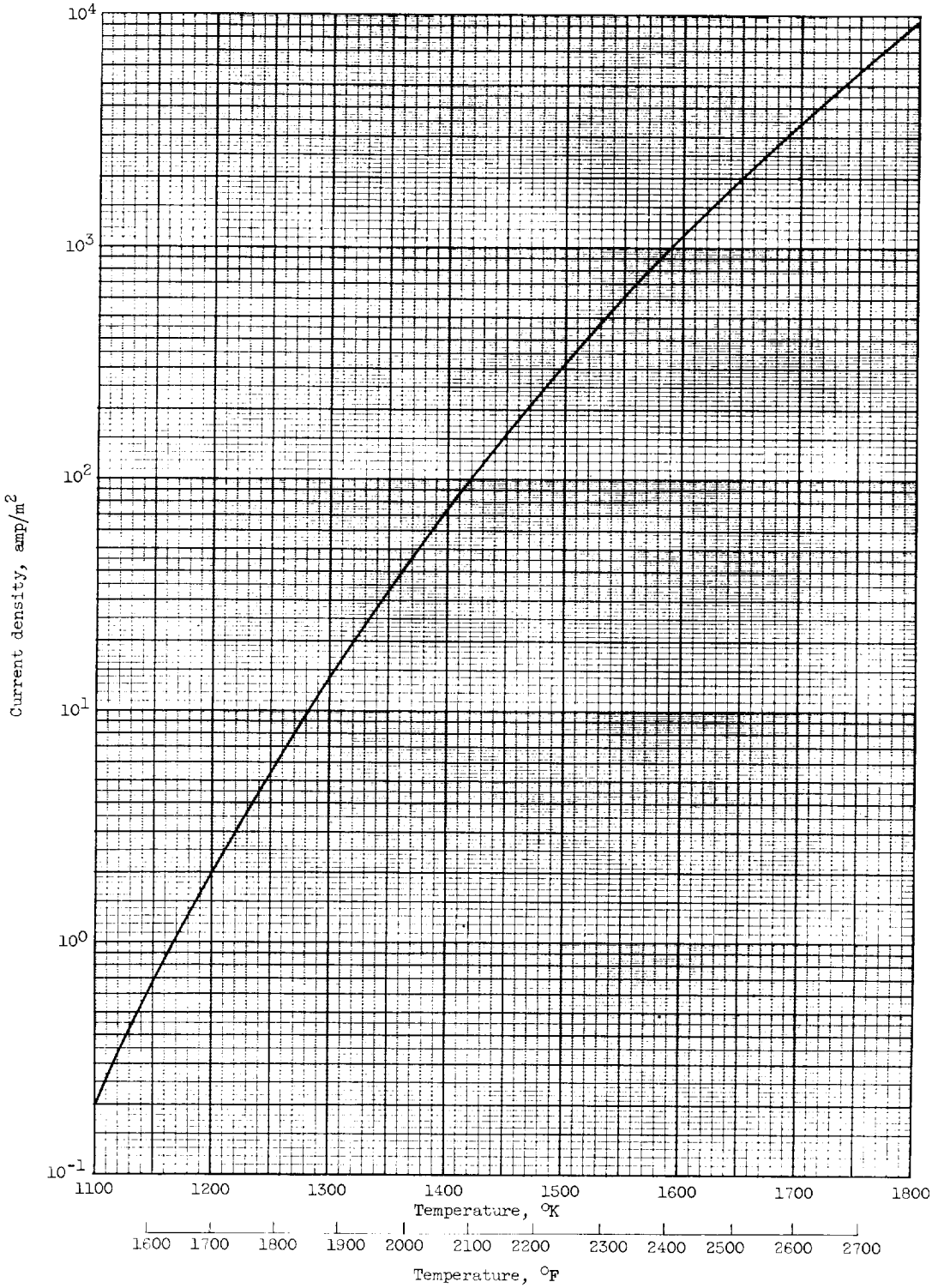

Figure 7. - Current - critical temperature relation (eq. (7)) for cesium on tungsten. $\log_{10} j = 11.3 - 13{,}200/T$.

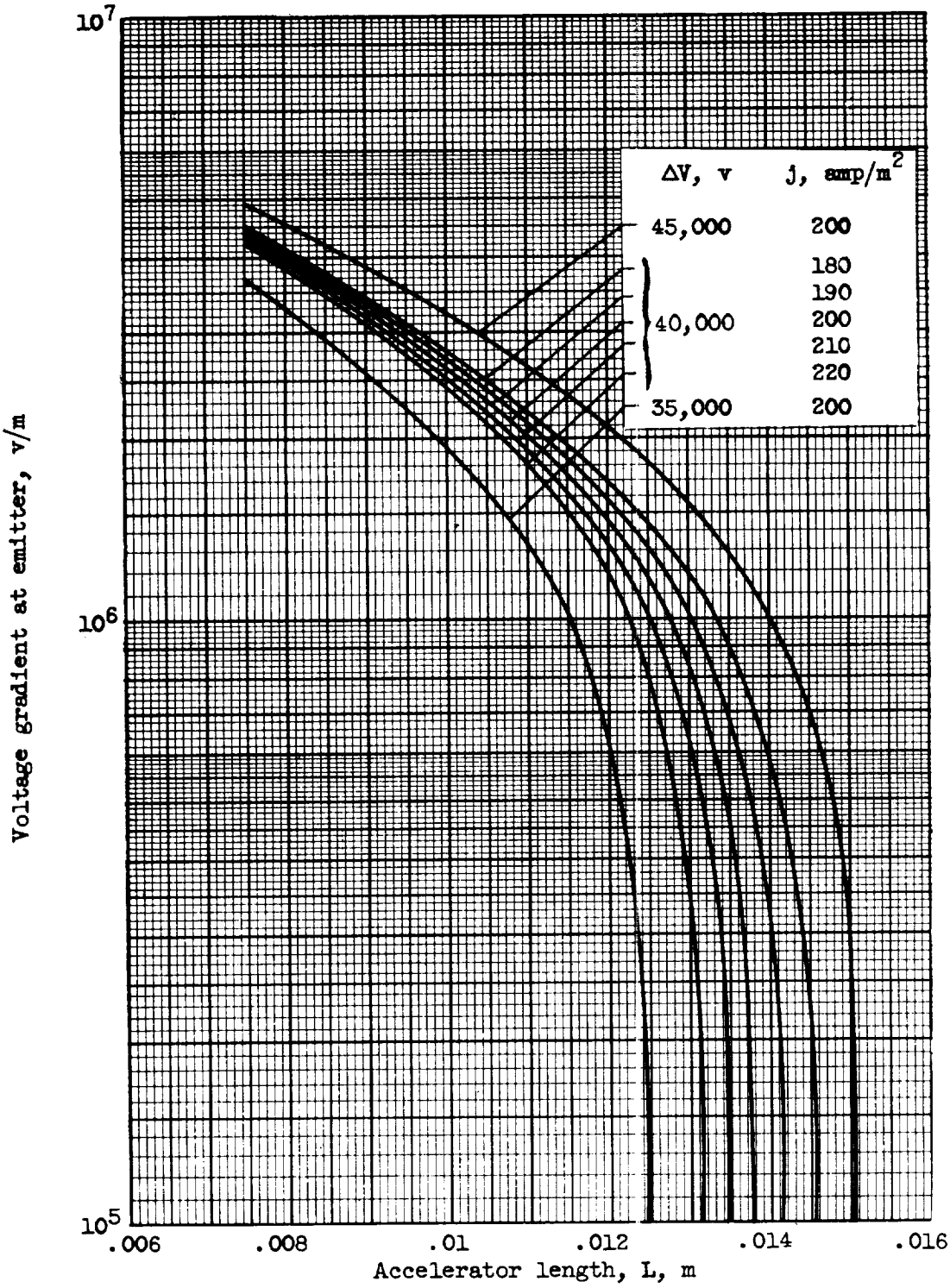

Figure 8. - Typical plot of voltage gradient at emitter with changes in accelerator length, voltage, and current (eq. (13)).

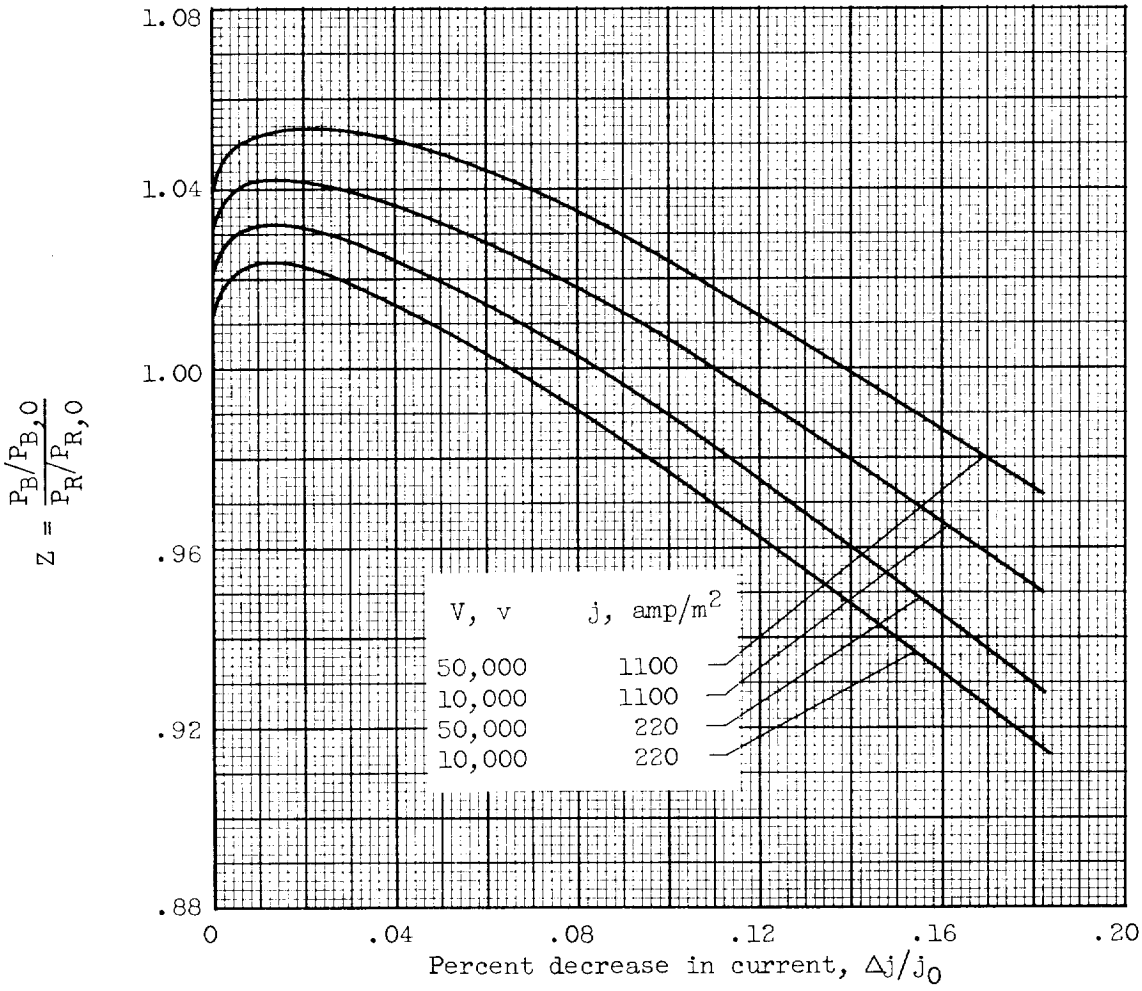

Figure 9. - Effect of operating off-space-charge conditions on ratio of beam power to radiated power.